

Strength of effective Coulomb interaction in two-dimensional transition-metal Halides MX_2 and MX_3 ($M=\text{Ti, V, Cr, Mn, Fe, Co, Ni}$; $X=\text{Cl, Br, I}$)

Y. Yekta,¹ H. Hadipour,^{1,*} E. Şaşıoğlu,^{2,†} C. Friedrich,^{3,‡} S. A. Jafari,^{4,§} S. Blügel,³ and I. Mertig²

¹*Department of Physics, University of Guilan, 41335-1914, Rasht, Iran*

²*Institute of Physics, Martin Luther University Halle-Wittenberg, 06120 Halle (Saale) Germany*

³*Peter Grünberg Institut and Institute for Advanced Simulation, Forschungszentrum Jülich and JARA, 52425 Jülich, Germany*

⁴*Department of Physics, Sharif University of Technology, Tehran 11155-9161, Iran*

(Dated: November 7, 2021)

We calculate the strength of the effective onsite Coulomb interaction (Hubbard U) in two-dimensional (2D) transition-metal (TM) dihalides MX_2 and trihalides MX_3 ($M=\text{Ti, V, Cr, Mn, Fe, Co, Ni}$; $X=\text{Cl, Br, I}$) from first principles using the constrained random-phase approximation. The correlated subspaces are formed from t_{2g} or e_g bands at the Fermi energy. Elimination of the efficient screening taking place in these narrow bands gives rise to sizable interaction parameters U between the localized t_{2g} (e_g) electrons. Due to this large Coulomb interaction, we find $U/W > 1$ (with the band width W) in most TM halides, making them strongly correlated materials. Among the metallic TM halides in paramagnetic state, the correlation strength U/W reaches a maximum in NiX_2 and CrX_3 with values much larger than the corresponding values in elementary TMs and other TM compounds. Based on the Stoner model and the calculated U and J values, we discuss the tendency of the electron spins to order ferromagnetically.

PACS numbers: 71.27.+a, 71.15.-m, 75.10.Lp, 68.90.+g

I. INTRODUCTION

Since the discovery of graphene [1, 2] two-dimensional (2D) materials have been extensively studied due to their rich physical properties and diverse technological applications. One of the important applications is the use of such 2D systems in spintronics for logic and memory applications [3–5]. In particular, 2D half-metallic magnets and spin-gapless semiconductors are desired for reconfigurable spintronic devices, which combines memory and logic into a single device [6]. Despite substantial interest, most of the 2D materials are, however, not magnetic in their pristine form. From a theoretical point of view, according to the Mermin-Wagner theorem [7], long-range magnetic order is not possible in 2D systems at finite temperatures, but this restriction is removed by magnetic anisotropy, which enables the formation of long-range magnetic order even in monolayers. Several standard approaches such as adsorption of atoms [8–12], point defects [13–17], and edge engineering [18–22] were developed to induce ferromagnetism in graphene and other graphene-like 2D materials. But these systematic ways are not well controlled for realistic applications. Therefore, 2D materials with intrinsic magnetism are of great interest for testing theories of magnetism in low dimensions as well as for ultralow-power memory and logic device applications.

Recently, intrinsic 2D ferromagnetism has been observed in materials containing transition-metal (TM) atoms such as in $\text{Cr}_2\text{Ge}_2\text{Te}_6$ [23], Fe_3GeTe_2 , CrI_3 [24–28], VSe_2 [29], and MnSe_2 [30]. For instance, it was observed that the CrI_3 monolayer exhibits ferromagnetic order below $T_c=45$ K [24]. VSe_2

and MnSe_2 were reported to have itinerant ferromagnetic order even at room temperature [29, 30]. Indeed, the synthesis of the CrI_3 monolayer has led to a huge experimental and theoretical interest. First-principles theoretical studies have predicted that the long-range magnetic order is also possible in other 2D monolayers of TM dihalides and trihalides (MX_2 and MX_3 , $M = \text{V, Cr, Mn, Fe and Ni}$, and $X=\text{Cl, Br and I}$) [31–41]. Besides CrI_3 , ferromagnetic order in the other TM halides such as CrCl_3 [42], CrBr_3 [43, 44], NiI_2 [45], and VI_3 [46, 47] monolayers were discovered experimentally and confirmed theoretically [48, 50–53].

Due to the presence of narrow t_{2g} or e_g states at the Fermi level [34] as well as reduced screening and quantum confinement effects arising from reduced dimensionality, correlation effects are expected to play a crucial role in determining the electronic and magnetic properties of the 2D TM halides. Density functional theory (DFT) based on the local-spin-density approximation (LSDA) or generalized gradient approximation (GGA) may therefore not be a reliable method to calculate the physical properties of TM halides. In this respect, methods beyond DFT such as DFT+ U and DFT+DMFT might be necessary. Some TM halides have been studied by employing the DFT+ U method [39, 41, 53], in which the effective Coulomb interaction parameters U are chosen arbitrarily or the U values of the 3D TMs are used. Only recently, a self-consistent constrained DFT method within linear response theory has been employed to calculate Hubbard U parameters for VCl_3 , VI_3 and CrX_3 ($X=\text{Cl, Br, I}$) [51, 52]. The obtained U parameters for V and Cr $3d$ orbitals turn out to be close to the corresponding values in elementary transition metals and other TM compounds [54, 55].

The aim of this paper is a first-principles determination of the strength of the effective Coulomb interaction (Hubbard U) between localized electrons in 2D TM halides MX_2 and MX_3 ($M = \text{V, Cr, Mn, Fe and Ni}$, and $X = \text{Cl, Br and I}$) by employing the constrained random-phase approximation

* hanifhadipour@gmail.com

† ersoy.sasioglu@physik.uni-halle.de

‡ c.friedrich@fz-juelich.de

§ jafari@sharif.edu

(cRPA) approach [56–58] within the full-potential linearized augmented plane-wave (FLAPW) method using maximally localized Wannier functions (MLWFs) [59, 60]. We find the Hubbard U parameters for t_{2g} or e_g electrons in metallic TM halides (paramagnetic state) vary between 1.0 and 5.1 eV, giving correlation strengths $U/W > 1$, larger than corresponding values in elementary TMs and other TM compounds demonstrating strong electronic correlation in the TM halides. Furthermore, based on the Stoner model, we use the calculated U and J values to assess the stability of the ferromagnetic ordering.

The rest of the paper is organized as follows: In Sec. II we briefly present the computational method and the cRPA method. In Sec. III, we present calculated values of Coulomb interaction parameters for MX_2 and MX_3 for TM halides. Finally, we summarize our conclusions in Sec. IV.

II. COMPUTATIONAL METHOD

We consider 2D TM halides with formulas MX_2 and MX_3 (M =Ti, V, Cr, Mn, Fe, Co, Ni; X =Cl, Br, I). Fig. 1(a) and Fig. 1(b) show the side and top view of crystal structures MX_2 dihalides and MX_3 trihalides, respectively. The lattice of TM dihalides consists of triangular nets of TM atoms and exhibits geometrical frustration when the magnetic moments couple antiferromagnetically. On the other hand, the TM atoms form honeycomb nets in MX_3 trihalide monolayers. The lattice parameters are taken from Refs. [33, 38, 39]. Simulation of MX_2 and MX_3 unit cells, containing one and two formula units, respectively, is based on the slab model having a 25 Å vacuum separating them. For DFT calculations we use the FLEUR code [61], which is based on the FLAPW method. For the exchange correlation functional we use the generalized gradient approximation (GGA) parametrized by Perdew *et al.* [62] (PBE). A $18 \times 18 \times 1$ k-point grid is used for all systems. A linear momentum cutoff of $G_{max} = 4.5 \text{ bohr}^{-1}$ is chosen for the plane waves. The effective Coulomb interaction parameters are calculated within the cRPA method [56–58] implemented in the SPEX code [64] with Wannier orbitals constructed from projection onto localized muffin-tin orbitals [60]. A dense $16 \times 16 \times 1$ k-point grid is used for the cRPA calculations.

To identify the correlated subspace and construct Wannier functions properly, non-spin-polarized projected density of states (DOS) are calculated for all systems and MLWFs are constructed for t_{2g} or e_g orbitals. To verify the validity of the calculated Wannier functions, in Fig. 2a(a) and Fig. 2b(b) we present a comparison of the non-spin-polarized DFT-PBE band structures with the corresponding Wannier-interpolated band structures obtained with e_g and t_{2g} Wannier orbitals for NiI_2 and CrI_3 , respectively. In all cases, the original and the Wannier-interpolated bands agree very well. The bands around the Fermi energy, formed by $\text{Ni-}e_g$ ($\text{Cr-}t_{2g}$) orbitals in NiI_2 (CrI_3), are well separated from the rest of the bands. They can thus be employed to define an effective two-orbital (six-orbital) low-energy Hamiltonian. In a similar fashion, correlated subspaces can be defined for all considered sys-

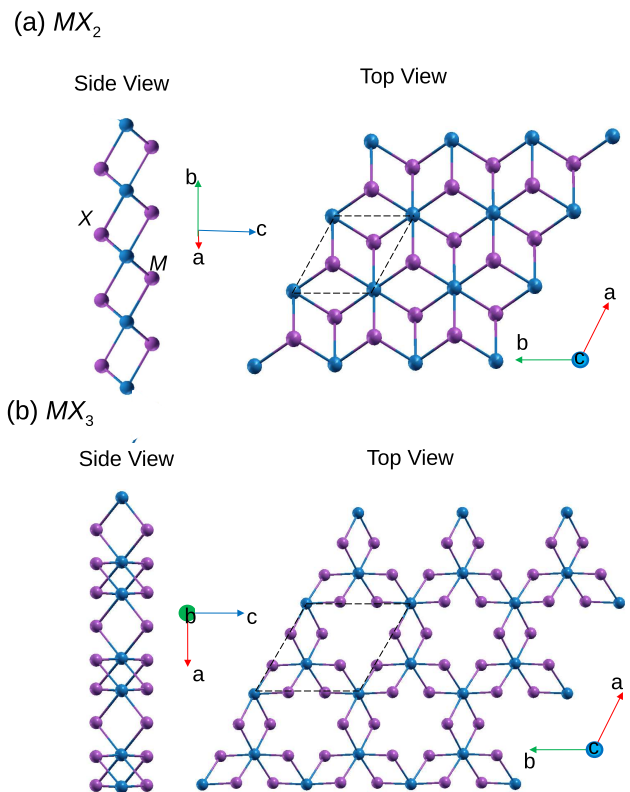


FIG. 1. (Colors online) (a) Top and side views of the two-dimensional crystal structure of TM dihalides MX_2 (b) Top and side views of the two-dimensional crystal structure of TM trihalides MX_3 . The blue and purple circles exhibit M and X atoms respectively. The M atoms in (a) form a frustrated triangular lattice, while in (b) their honeycomb structure is a bi-partite and hence non-frustrated lattice.

tems, of t_{2g} and e_g character for early and late TM halides, respectively, as shown in Fig. 3. We note that the t_{2g} - e_g splitting is small for some systems (in particular, for some of the dihalides)[65]. It could, therefore, be necessary to go beyond the present minimal subspace by including, for example, the full d shell or by considering spin polarization. However, it is already obvious from Fig. 3 that one might then encounter the problem of entangled bands, which, on the one hand, complicates the Wannier construction and, on the other, makes the elimination of the subspace screening Eq. (4) less straightforward. For the present comparative study of the electron-electron interaction strength in a large class of materials, we therefore restrict ourselves to the minimal subspaces, all formed by isolated sets of bands, which will capture the essential physics of these materials. Our calculations may serve as reference point for more sophisticated studies of any of the investigated materials in the future.

Due to the systems' symmetry, the bands are not of pure t_{2g} and e_g character but are mixtures and also exhibit admixture from I - p states. The denomination " t_{2g} " and " e_g " thus refers to their dominant orbital character. We describe the orbitals in more detail in the following.

In all systems, the TM atoms are each bound to six halo-

gen atoms in octahedral coordination. The octahedron is, however, tilted with respect to the standard cartesian coordinate system, which has the z -axis perpendicular to the layers. Furthermore, the octahedron is distorted because of the two-dimensionality of the structure. Opposite halogens are still exactly opposite (forming a halogen-TM-halogen bond angle of 180°), whereas of the remaining twelve halogen-TM-halogen bond angles six are slightly below and six are slightly above 90° . For example, in NiI_2 (CrI_3) the difference to the right angle is 8.62° (1.13°).

The octahedron is tilted in such a way that two opposite faces of the octahedron are parallel to the layers. If we take the three Ni-I bonds in NiI_2 , whose iodine ends form the corners of one of these octahedron faces, as x' -, y' - and z' -axes, we can identify local e_g orbitals in Fig. 2b(c). The orbitals show a strong admixture of iodine p states, a delocalization effect which will be reflected in reduced interaction parameters later-on. Still, the d_{z^2} and $d_{x'^2-y'^2}$ orbital character is readily seen. In CrI_3 , the octahedron is similarly tilted, and we can consider local x' -, y' -, z' -axes as above. While two of the orbitals presented in Fig. 2b(d) indeed look like t_{2g} orbitals, the one in the middle actually has the form of a d_{z^2} orbital, which is, however, oriented along the cartesian z -axis, perpendicular to the layers. In fact, if we linearly combine the local t_{2g} orbitals by $(d_{x'y'} + d_{y'z'} + d_{x'z'})/\sqrt{3}$, we obtain a d_{z^2} orbital oriented perpendicular to the layer. This linear combination results from the breaking of octahedral symmetry caused by the layer structure. The other two t_{2g} orbitals, $(d_{y'z'} - d_{x'y'})/\sqrt{2}$ and $(d_{x'y'} + d_{y'z'} - 2d_{x'z'})/\sqrt{6}$, can be described, respectively, as a $d_{x'y'}$ rotated by 45° around the y -axis and a distorted $d_{x'z'}$ orbital.

The fully screened Coulomb interaction \tilde{U} is related to the bare Coulomb interaction V by

$$\tilde{U}(\mathbf{r}, \mathbf{r}', \omega) = \int d\mathbf{r}'' \epsilon^{-1}(\mathbf{r}, \mathbf{r}'', \omega) V(\mathbf{r}'', \mathbf{r}'), \quad (1)$$

where $\epsilon(\mathbf{r}, \mathbf{r}'', \omega)$ is the dielectric function. The dielectric function is related to the electron polarizability P by

$$\epsilon(\mathbf{r}, \mathbf{r}', \omega) = \delta(\mathbf{r} - \mathbf{r}') - \int d\mathbf{r}'' V(\mathbf{r}, \mathbf{r}'') P(\mathbf{r}'', \mathbf{r}', \omega), \quad (2)$$

where the RPA polarization function $P(\mathbf{r}'', \mathbf{r}', \omega)$ is given by

$$P(\mathbf{r}, \mathbf{r}', \omega) = 2 \sum_m^{\text{occ}} \sum_{m'}^{\text{unocc}} \varphi_m(\mathbf{r}) \varphi_{m'}^*(\mathbf{r}) \varphi_{m'}^*(\mathbf{r}') \varphi_m(\mathbf{r}') \times \left[\frac{1}{\omega - \Delta_{mm'} + i\eta} - \frac{1}{\omega + \Delta_{mm'} - i\eta} \right]. \quad (3)$$

Here, $\varphi_m(\mathbf{r})$ are the single-particle DFT Kohn-Sham eigenfunctions, and η a positive infinitesimal. $\Delta_{mm'} = \epsilon_{m'} - \epsilon_m$ with the Kohn-Sham eigenvalues ϵ_m . β

In the cRPA approach, in order to exclude the screening due to the correlated subspace, we separate the full polarization function of Eq. (3) into two parts

$$P = P_d + P_r, \quad (4)$$

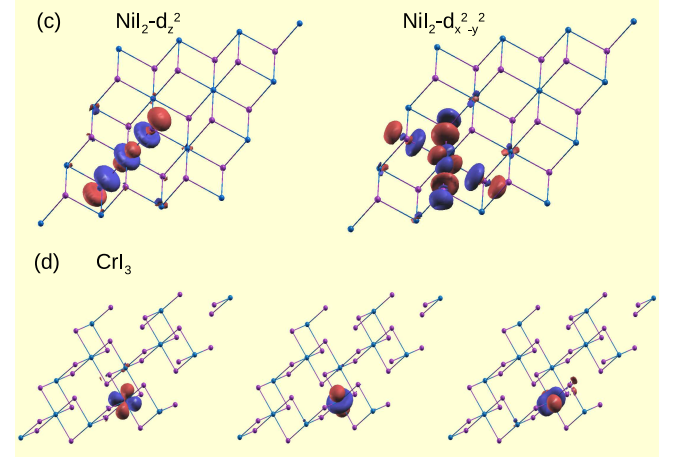
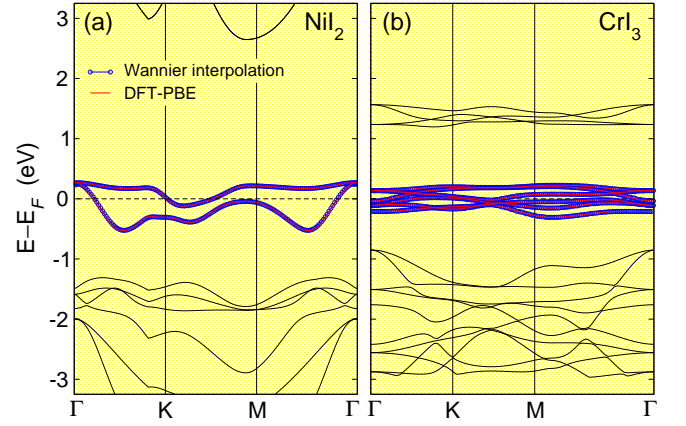


FIG. 2. (Color online) DFT-PBE (red) and Wannier-interpolated band structures (blue) of non-spin-polarized (a) NiI_2 and (b) CrI_3 . (c) The e_g -like MLWFs for Ni atoms of NiI_2 . (d) The t_{2g} -like MLWFs for Cr atoms of CrI_3 .

where P_d includes only the transitions ($m \rightarrow m'$) between the states of the correlated subspace and P_r is the remainder. Then, the frequency-dependent effective Coulomb interaction is given schematically by the matrix equation

$$U(\omega) = [1 - V P_r(\omega)]^{-1} V. \quad (5)$$

It contains, in P_r , screening processes that would not be captured by the correlated subspace and excludes the ones that take place within the subspace.

The matrix elements of the effective Coulomb interaction in the MLWF basis are given by

$$U_{\mathbf{R}n_1, n_3, n_2, n_4}(\omega) = \int \int d\mathbf{r} d\mathbf{r}' w_{n_1\mathbf{R}}^*(\mathbf{r}) w_{n_3\mathbf{R}}(\mathbf{r}) U(\mathbf{r}, \mathbf{r}', \omega) w_{n_4\mathbf{R}}^*(\mathbf{r}') w_{n_2\mathbf{R}}(\mathbf{r}'), \quad (6)$$

where $w_{n\mathbf{R}}(\mathbf{r})$ is the MLWF at site \mathbf{R} with orbital index n , and the effective Coulomb potential $U(\mathbf{r}, \mathbf{r}', \omega)$ is calculated within the cRPA as described above. We define the average Coulomb matrix elements U , U' , and J in the static limit ($\omega =$

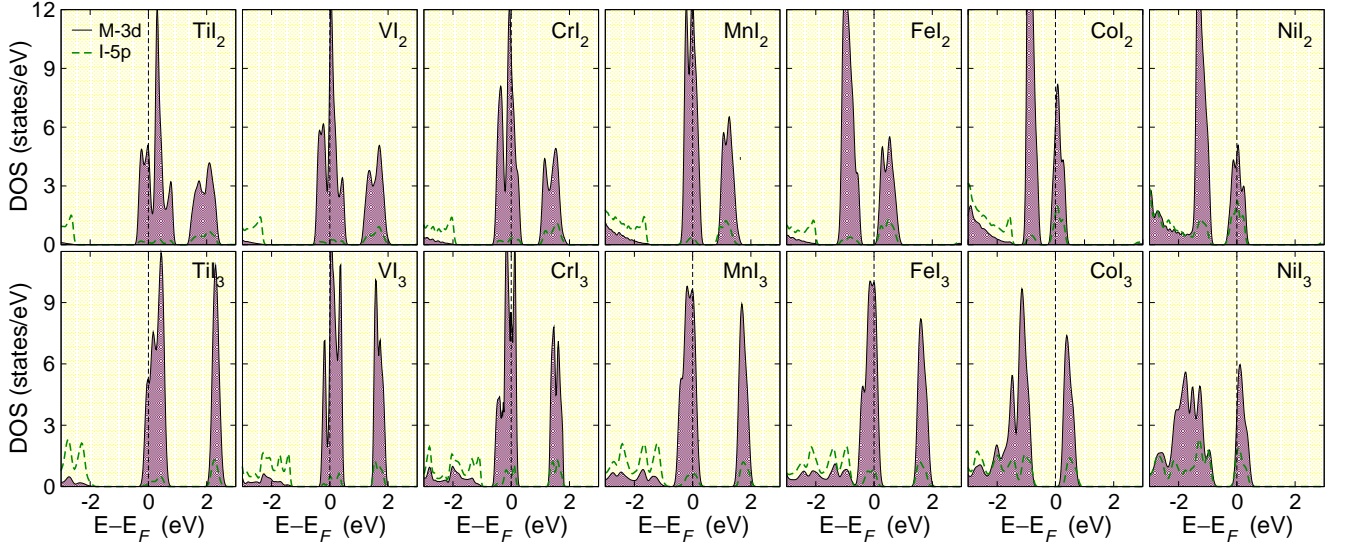


FIG. 3. (Colors online) Orbital-resolved DOS for the non-spin-polarized MI_2 and MI_3 TM halides. Each panel shows the DOS projected onto $3d$ states of the M atom as well as on $5p$ states of the I atom. The two distinct groups of d bands correspond to t_{2g} and e_g bands, respectively. The former overlaps with $5p$ states in the late TM iodides.

0) as follows [66, 67]:

$$U = \frac{1}{L} \sum_m U_{mm;mm}, \quad (7)$$

$$U' = \frac{1}{L(L-1)} \sum_{m \neq n} U_{mn;mn}, \quad (8)$$

$$J = \frac{1}{L(L-1)} \sum_{m \neq n} U_{mn;nm}, \quad (9)$$

where L is the number of localized orbitals, i.e., two for e_g and three for t_{2g} orbitals. This parametrization of partially screened Coulomb interactions is the so-called Hubbard-Kanamori parametrization. Similar to the definition of U (U' , J), we can also define the so-called fully screened interaction parameters \tilde{U} (\tilde{U}' , \tilde{J}) as well as unscreened (bare) V . The bare V provides information about the localization of Wannier functions and is a useful parameter in the interpretation of the screened Coulomb interaction parameters.

III. RESULTS AND DISCUSSION

In the low-energy model Hamiltonian description of correlated solids, the non-interacting one-electron part of the effective model is defined for a system, in which there is no spontaneous symmetry breaking, i.e., it is a paramagnetic (non-spin-polarized) metal. The calculation of effective Coulomb interaction parameters (Hubbard U) should therefore be based on such a system.

To identify the correlated subspace for all studied TM halides, we present in Fig. 3 orbital-resolved DOS for MI_2

and MI_3 . In all compounds except for the semiconducting FeI_2 and CoI_3 , the Fermi energy falls into a group of bands, which are of t_{2g} character for the early halides, $M = Ti$ to Mn (Ti to Fe) for MI_2 (MI_3), and of e_g character for the late halides, $M = Co$ and Ni (Ni) for MI_2 (MI_3). These bands are assumed to form minimal correlated subspaces in this work. On the other hand, FeI_2 and CoI_3 are semiconducting with the Fermi level falling in the energy gap between the t_{2g} and e_g bands. Depending on the type of doping, electron or hole doping, only one type of bands will form the minimal correlated subspace. For these systems, we will present Hubbard U parameters for t_{2g} , e_g , and d orbitals. The first two correspond to the zero-doping limit (or very dilute doping), since the states of the subspace are either all occupied or all empty. As hence no screening takes place in the subspace, the partially and fully screened parameters (e.g., U and \tilde{U}) are identical. The orbital-resolved DOS of MX_2 and MX_3 with $X = Cl$ and Br look very similar, so the subspaces can be defined identically to those of the iodides. The U matrix element of the p-admixed t_{2g} state differs from the pure t_{2g} state by maximally 0.1 eV among the materials. The calculated Hubbard U values should therefore be applicable to standard DFT+ U implementations that are based on atomic bases, as well, not only to implementations that employ Wannier functions.

In Table I, we present the onsite average intra-orbital unscreened (bare) Coulomb interaction V , partially (fully) screened U (\tilde{U}), as well as average inter-orbital U' (\tilde{U}') and exchange parameter J (\tilde{J}). The behavior of the bare interaction V for t_{2g} orbitals across the $3d$ TM atoms, from Ti to Fe , in MX_2 is similar to the case of elementary TMs. The V parameter increases nearly linearly with increasing electron number, which is due to the contraction of the wave functions with increased nuclear charge and the concomitant increased localization of the Wannier functions. By contrast, the e_g orbitals exhibit the opposite trend from Fe to Ni in MX_2 : The

V decreases. An analysis of the shape of the Wannier orbitals reveals that the coupling to neighboring halogen p states gets stronger, which makes the orbitals increasingly spill into these states giving rise to a delocalization and, therefore, to smaller V parameters. The same trend is seen for MX_3 from Co to Ni. The behavior of V for the t_{2g} orbitals in the trihalides is somewhat different from that of the dihalides: While early in the series from Ti to Co we see a similar increase as in the dihalides, the values go over a maximum and drop off sharply for CoX_3 . In all cases, we see a decrease of the bare V for the halide series MX_2 with $X = Cl$ to I , which is likely caused by the increase of the lattice constant in this order, making the orbitals more extended.

The effects are reflected also in the band widths W of the t_{2g} and e_g bands presented in Table I (also see Fig. 3), which tend to decrease from Ti to Ni, similar to the case of elementary $3d$ TMs with the difference that, due to reduced coordination (reduced hybridization) in 2D, the W is much smaller than the corresponding values in $3d$ TMs, making the t_{2g} and e_g peaks in the DOS sharper and more atomic-like.

To discuss the partially screened (Hubbard U) effective Coulomb interaction parameters, we focus on the TM iodides. As seen in Table I, the U values for M sites in MI_2 (MI_3) compounds vary between 2.1–3.3 eV (1.1–3.0 eV) and decrease with moving from Ti to Ni, which can be described by the projected density of states in Fig. 3. Just below the d states there is a broad peak of iodine $5p$ states, which should contribute with $5p \rightarrow d$ transitions sizably to the screening. Across the series Ti to Ni, the $5p$ states are seen to approach the d states, which effectively increases the electronic screening and, thus, acts to compensate the increase of U caused by Wannier localization, giving rise to the reduction of U parameters with increasing $3d$ electron number in both types of TM halides. The same behaviour is observed in Br- and Cl-based TM halides (see Table I).

Moving upwards in the group of halogens, from I to Cl , the $M-X$ bond lengths decrease. As a consequence, orbitals overlap more strongly and hybridization increases, pushing the states apart energetically. The larger energy difference makes electronic transitions $p \rightarrow t_{2g}$ less likely and reduces electronic screening. From this, one would expect to see a tendency to larger Hubbard U values, which is, in fact, what we observe in Table I.

Comparing the partially screened (U) with the fully screened parameters (\tilde{U}) gives information about the screening within the correlated subspace. Except for the semiconductors FeM_2 and CoM_3 , this screening is metallic. It is very efficient and becomes the dominant screening channel. As a consequence, the fully screened parameters \tilde{U} show a behavior very different from U : The values are all very small for the metallic systems and fall in the range between 0.1 and 0.5 eV, about one fifth of the U values. They do not follow a specific trend across the TM series, nor do they follow a general ordering with respect to the different kinds of halides (Cl , Br , I) as in the partially screened U parameters. Our results show that $t_{2g} \rightarrow t_{2g}$ and $e_g \rightarrow e_g$ transitions contribute substantially to the screening of the fully screened Coulomb interaction \tilde{U} in metallic systems, while in the semiconducting ones

this screening vanishes, making \tilde{U} identical to U for the t_{2g} and e_g orbitals, whereas the $t_{2g} \rightarrow e_g$ transitions reduce \tilde{U} with respect to U for the full $3d$ shell.

In the semiconducting cases FeX_2 and CoX_3 , the $3d$ parameters show a behavior parallel to that of the t_{2g}/e_g parameters and are larger by about 20-70%, elucidating that transitions between t_{2g} and e_g states play an important quantitative role in the electronic screening but do not affect the screening qualitatively.

In cubic symmetry, the Hubbard-Kanamori inter-orbital Coulomb interaction term U' satisfies the relation $U' = U - 2J$. This relation is nearly fulfilled in most TM halides, even though cubic symmetry is broken. The J parameters vary in the range 0.20–0.57 eV and show a behavior very much in parallel to the bare parameters V , despite the very different range of values, which reveals a more quantitative than qualitative effect of the electronic screening on the exchange parameters J .

We now compare our calculated Hubbard U values with reported ones in the literature. Besbes et al. [48] calculated Hubbard U values for bulk $CrCl_3$ and CrI_3 and obtained U values of 1.79 eV ($CrCl_3$) and 1.15 eV (CrI_3), which are significantly smaller than our calculated Coulomb matrix elements presented in Table I, whereas their exchange parameters are larger (0.85 and 0.78 eV) than our values. A possible reason for the disagreement is the different dimensionality of the systems, 3D versus 2D. 3D materials usually offer more screening with the consequence of smaller U parameters. There are other possible reasons: Besbes et al. employ a method different to ours, a combined cLDA/RPA scheme [49]. They also used a different Wannier basis. They combined chromium d and halogen p states into a larger Wannier basis for a dp tight-binding description, whereas we have employed minimal t_{2g} and e_g subspaces. And, finally, the definition of the Hubbard U parameter is different. We have calculated Hubbard-Kanamori parameters for the t_{2g} and e_g subsets (see Eq. (7)), whereas Besbes et al. defined the Hubbard parameters for the full atomic p and d shells. In this different kind of U parameter the averaging is over the full matrix instead of just over the diagonal elements.

In the case of V-based trihalides, He et al. calculated U values for VCl_3 and VI_3 using the self-consistent linear response method within the cLDA approach and obtained $U=3.35$ eV (for VCl_3) and 3.68 eV (for VI_3) [51]. These values are closer to our results.

In the following, we discuss the appearance of ferromagnetism in TM halides. The ferromagnetic state is the ground state for most of the TM trihalides MX_3 , while TM dihalides MX_2 exhibit diverse magnetic behavior ranging from half-metallic ferromagnetism ($FeCl_2$) to antiferromagnetism (VI_2) and from 120° -antiferromagnetism (MnI_2) to helical magnetism (NiI_2). A richness of magnetic phases that results from the triangular lattice of M atoms, which frustrates the exchange coupling. Such a frustration is not present for MX_3 compounds, where M atoms reside on a bi-partite (honeycomb) lattice. The calculation of U parameters for such complex magnetic ground states is beyond the scope of the present paper. Note that such a calculation would require the full $3d$

TABLE I. Lattice constants a , orbital type of correlated subspace, bandwidth W , onsite average intra-orbital bare V , partially (fully) screened U (\tilde{U}), inter-orbital partially (fully) screened U' (\tilde{U}'), partially (fully) screened exchange interaction J (\tilde{J}), correlation strength U/W , and the DOS at the Fermi level $D(E_F)$ for MX_2 and MX_3 compounds.

| $MX_{2/3}$ | a (Å) | orbitals | W (eV) | V (eV) | U (\tilde{U}) (eV) | U' (\tilde{U}') (eV) | J (\tilde{J}) (eV) | U/W | $D(E_F)$ |
|-------------------|---------|----------|----------|----------|--------------------------|----------------------------|--------------------------|-------|----------|
| TiCl ₂ | 3.56 | t_{2g} | 1.43 | 14.07 | 5.07 (0.87) | 4.22 (0.43) | 0.43 (0.23) | 3.55 | 0.45 |
| TiBr ₂ | 3.73 | t_{2g} | 1.31 | 13.32 | 4.26 (0.79) | 3.47 (0.41) | 0.39 (0.19) | 3.25 | 0.51 |
| TiI ₂ | 4.11 | t_{2g} | 1.15 | 11.70 | 3.26 (0.63) | 2.61 (0.32) | 0.33 (0.16) | 2.83 | 0.73 |
| VCl ₂ | 3.62 | t_{2g} | 1.20 | 15.95 | 4.60 (0.95) | 3.62 (0.63) | 0.51 (0.16) | 3.83 | 1.28 |
| VBr ₂ | 3.81 | t_{2g} | 1.03 | 14.96 | 3.98 (0.86) | 3.03 (0.57) | 0.49 (0.16) | 3.86 | 1.91 |
| VI ₂ | 4.08 | t_{2g} | 0.94 | 13.63 | 3.10 (0.44) | 2.33 (0.27) | 0.39 (0.10) | 3.30 | 2.25 |
| CrCl ₂ | 3.55 | t_{2g} | 1.05 | 17.32 | 4.13 (0.23) | 3.13 (0.03) | 0.54 (0.09) | 3.93 | 4.50 |
| CrBr ₂ | 3.74 | t_{2g} | 0.99 | 16.51 | 3.64 (0.23) | 2.68 (0.06) | 0.51 (0.08) | 3.68 | 4.87 |
| CrI ₂ | 3.99 | t_{2g} | 0.96 | 14.88 | 2.96 (0.26) | 2.16 (0.07) | 0.42 (0.10) | 3.08 | 3.64 |
| MnCl ₂ | 3.64 | t_{2g} | 0.85 | 19.10 | 3.71 (0.82) | 2.69 (0.62) | 0.56 (0.08) | 4.36 | 6.41 |
| MnBr ₂ | 3.84 | t_{2g} | 0.81 | 18.12 | 3.25 (0.29) | 2.29 (0.06) | 0.52 (0.07) | 4.01 | 6.02 |
| MnI ₂ | 4.12 | t_{2g} | 0.75 | 17.19 | 2.76 (0.26) | 1.90 (0.04) | 0.46 (0.06) | 3.68 | 4.18 |
| FeCl ₂ | 3.49 | t_{2g} | 1.10 | 20.11 | 3.50 (3.50) | 2.43 (2.43) | 0.56 (0.56) | 3.18 | 0.00 |
| | | e_g | 0.70 | 17.00 | 3.06 (3.06) | 2.06 (2.06) | 0.50 (0.50) | 4.37 | 0.00 |
| | | d | 2.41 | 19.96 | 5.97 (3.21) | 4.84 (2.42) | 0.57 (0.42) | 2.48 | 0.00 |
| FeBr ₂ | 3.69 | t_{2g} | 0.97 | 19.02 | 3.14 (3.14) | 2.11 (2.11) | 0.53 (0.53) | 3.24 | 0.00 |
| | | e_g | 0.78 | 15.24 | 2.64 (2.64) | 1.76 (1.76) | 0.44 (0.44) | 3.38 | 0.00 |
| | | d | 2.37 | 19.13 | 5.21 (3.07) | 3.86 (2.20) | 0.55 (0.42) | 2.20 | 0.00 |
| FeI ₂ | 3.98 | t_{2g} | 0.80 | 17.39 | 2.52 (2.52) | 1.66 (1.66) | 0.44 (0.44) | 3.15 | 0.00 |
| | | e_g | 0.91 | 12.83 | 2.03 (2.03) | 1.36 (1.36) | 0.33 (0.33) | 2.23 | 0.00 |
| | | d | 2.21 | 17.64 | 4.07 (3.05) | 2.98 (1.67) | 0.53 (0.38) | 1.84 | 0.00 |
| CoCl ₂ | 3.49 | e_g | 0.59 | 16.51 | 3.18 (0.38) | 2.20 (0.26) | 0.49 (0.06) | 5.39 | 3.26 |
| CoBr ₂ | 3.73 | e_g | 0.61 | 14.93 | 2.67 (0.19) | 1.82 (0.07) | 0.42 (0.06) | 4.38 | 3.51 |
| CoI ₂ | 3.92 | e_g | 0.64 | 12.26 | 2.16 (0.16) | 1.52 (0.03) | 0.32 (0.07) | 3.38 | 4.54 |
| NiCl ₂ | 3.45 | e_g | 0.53 | 15.17 | 3.37 (0.16) | 2.43 (0.04) | 0.47 (0.06) | 6.36 | 4.12 |
| NiBr ₂ | 3.64 | e_g | 0.59 | 13.52 | 3.09 (0.22) | 2.27 (0.07) | 0.41 (0.07) | 5.24 | 3.28 |
| NiI ₂ | 3.94 | e_g | 0.62 | 10.60 | 2.36 (0.44) | 1.78 (0.27) | 0.29 (0.09) | 3.81 | 2.76 |
| TiCl ₃ | 5.88 | t_{2g} | 1.16 | 14.48 | 4.62 (0.68) | 3.75 (0.24) | 0.46 (0.22) | 3.98 | 1.09 |
| TiBr ₃ | 6.27 | t_{2g} | 1.08 | 14.15 | 3.97 (0.51) | 3.12 (0.16) | 0.43 (0.17) | 3.68 | 0.82 |
| TiI ₃ | 6.62 | t_{2g} | 1.01 | 12.86 | 2.99 (0.37) | 2.26 (0.06) | 0.38 (0.15) | 2.96 | 0.61 |
| VCl ₃ | 6.04 | t_{2g} | 0.91 | 16.28 | 4.49 (0.31) | 3.46 (0.04) | 0.54 (0.14) | 4.93 | 1.17 |
| VBr ₃ | 6.33 | t_{2g} | 0.86 | 15.59 | 3.82 (0.36) | 2.84 (0.09) | 0.51 (0.14) | 4.44 | 1.86 |
| VI ₃ | 6.86 | t_{2g} | 0.82 | 14.47 | 2.91 (0.28) | 2.07 (0.06) | 0.44 (0.12) | 3.55 | 2.44 |
| CrCl ₃ | 5.75 | t_{2g} | 0.81 | 16.53 | 4.08 (0.48) | 3.07 (0.20) | 0.53 (0.17) | 5.04 | 2.72 |
| CrBr ₃ | 6.34 | t_{2g} | 0.76 | 16.24 | 3.50 (0.31) | 2.52 (0.12) | 0.51 (0.10) | 4.61 | 2.40 |
| CrI ₃ | 6.85 | t_{2g} | 0.61 | 15.29 | 2.67 (0.25) | 1.84 (0.10) | 0.44 (0.08) | 4.38 | 2.47 |
| MnCl ₃ | 6.08 | t_{2g} | 0.85 | 18.05 | 3.64 (0.56) | 2.63 (0.30) | 0.55 (0.13) | 4.28 | 2.15 |
| MnBr ₃ | 6.39 | t_{2g} | 0.79 | 17.28 | 3.15 (0.55) | 2.19 (0.31) | 0.51 (0.13) | 3.99 | 3.19 |
| MnI ₃ | 6.85 | t_{2g} | 0.65 | 15.73 | 2.62 (0.48) | 1.61 (0.26) | 0.44 (0.12) | 4.03 | 3.39 |
| FeCl ₃ | 6.05 | t_{2g} | 0.82 | 18.14 | 3.30 (0.33) | 2.32 (0.14) | 0.54 (0.09) | 4.02 | 2.52 |
| FeBr ₃ | 6.43 | t_{2g} | 0.78 | 17.24 | 2.85 (0.29) | 1.92 (0.11) | 0.50 (0.09) | 3.65 | 2.47 |
| FeI ₃ | 6.97 | t_{2g} | 0.69 | 15.29 | 2.14 (0.22) | 1.37 (0.03) | 0.41 (0.08) | 3.10 | 2.62 |
| CoCl ₃ | 6.07 | t_{2g} | 0.65 | 16.82 | 2.95 (2.95) | 2.05 (2.05) | 0.50 (0.50) | 4.54 | 0.00 |
| | | e_g | 0.45 | 13.95 | 2.43 (2.43) | 1.67 (1.67) | 0.38 (0.38) | 5.40 | 0.00 |
| | | d | 1.72 | 16.21 | 3.60 (2.70) | 2.67 (2.04) | 0.47 (0.35) | 2.09 | 0.00 |
| CoBr ₃ | 6.30 | t_{2g} | 0.93 | 14.47 | 2.45 (2.45) | 1.67 (1.67) | 0.43 (0.43) | 2.63 | 0.00 |
| | | e_g | 0.78 | 12.84 | 2.11 (2.11) | 1.42 (1.42) | 0.34 (0.34) | 2.71 | 0.00 |
| | | d | 2.45 | 14.27 | 3.08 (2.23) | 2.26 (1.71) | 0.39 (0.31) | 1.26 | 0.00 |
| CoI ₃ | 6.81 | t_{2g} | 1.62 | 10.34 | 1.34 (1.34) | 0.94 (0.94) | 0.24 (0.24) | 0.83 | 0.00 |
| | | e_g | 1.10 | 10.92 | 1.48 (1.48) | 0.96 (0.96) | 0.26 (0.26) | 1.35 | 0.00 |
| | | d | 3.32 | 10.65 | 2.10 (1.40) | 1.55 (1.05) | 0.24 (0.18) | 0.63 | 0.00 |
| NiCl ₃ | 6.05 | e_g | 0.63 | 11.76 | 2.01 (0.15) | 1.39 (0.04) | 0.31 (0.06) | 3.19 | 2.52 |
| NiBr ₃ | 6.16 | e_g | 0.75 | 10.55 | 1.79 (0.25) | 1.22 (0.11) | 0.28 (0.07) | 2.39 | 1.85 |
| NiI ₃ | 6.64 | e_g | 0.91 | 8.55 | 1.08 (0.24) | 0.69 (0.10) | 0.20 (0.07) | 1.19 | 1.40 |

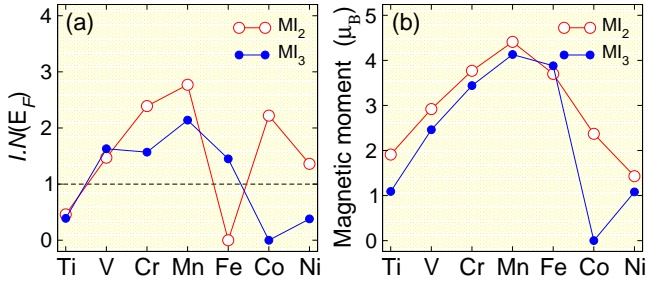


FIG. 4. (Colors online) (a) Stoner criterion for MI_2 and MI_3 TM halides. (b) Calculated magnetic moments (in units of μ_B) of TM atoms for MI_2 and MI_3 TM halides.

shell to be included in the correlated subspace. The present values for the minimal t_{2g} and e_g subspaces would not be immediately applicable in this case.

Among the TM trihalides, CrI_3 is of particular interest for spintronic applications as well as theories of low-dimensional magnetism because it was one of the first materials in which ferromagnetism was detected experimentally in the monolayer limit. It is a ferromagnetic semiconductor with a Curie temperature of 45 K in the monolayer and 61 K in the bulk.

As the MX_2 and MX_3 halides contain partially filled $3d$ TM atoms, we can use the simple Stoner model to discuss the appearance of ferromagnetism in these materials. The Stoner criterion for ferromagnetism is given by $I \cdot D(E_F) > 1$, where I is the Stoner parameter and $D(E_F)$ is the DOS at the Fermi energy in the nonmagnetic state. The Hartree-Fock solution of the multiorbital Hubbard model gives a relationship between the Stoner parameter I , Hubbard U , and exchange J by $I = (U + 6J)/5$ [68]. Stollhoff et al. showed that in elementary TMs the electron correlations reduce I by roughly 40%. We note that the magnetism in some of the TM halides might not be describable by the simple Stoner mechanism. For example, MnI_2 has an antiferromagnetic (120 degrees) ground state. For reasons of consistency, we nevertheless discuss the Stoner condition for all materials and leave more detailed analyses taking into account Hund's rule coupling for future studies. In Fig. 4 (a) we present the correspondingly scaled Stoner parameter $I \cdot D(E_F)$ for iodine-based compounds. The experimentally observed and theoretically predicted ferromagnetic TM halides satisfy the Stoner criterion, and the paramagnetic state is unstable toward the formation of ferromagnetism, which reasonably agrees with the results of spin-polarized DFT total energy calculations and the large magnetic moments presented in Fig. 4(b). The failure of the Stoner criterion to predict the ferromagnetism of FeI_2 is due to the fact that this compound is a semiconductor, while the Stoner criterion is based on a metallic parent (non-interacting) limit.

With this tendency to form magnetic ground states, one might wonder whether and to what degree the Hubbard U parameters would change if a magnetic ground state were taken as reference system instead of the non-spin-polarized one. For instance for the case of MnI_2 , we obtain a U value of 3.37 eV, which is not too different from the paramagnetic case (2.76 eV). This might be due to the fact that the formation of

the magnetic moments predominantly affects the low-energy states, but these are just the ones that make up the correlated subspace whose screening channels are eliminated from the effective Hubbard U interaction.

Finally, we want to briefly discuss the strength of the electronic correlations in 2D TM halides. Qualitatively, the correlation strength is defined as the ratio of the effective Coulomb interaction U to the bandwidth W (U/W). In Table I we present U/W values for all TM halides. Note that the U/W values are calculated for a non-spin-polarized (paramagnetic) state. In the case of MX_2 and ignoring the non-metallic system (FeX_2), the correlation strength U/W tends to increase from Ti- to Ni-based materials. There is no clear trend in the trihalides, although a strong decrease of U/W is noted for the e_g subspace in the iodides and, less pronounced, also in the bromides. For most of the metallic TM halides, we find $U/W > 2$ with maxima for $NiCl_2$ and $CrCl_3$. We thus expect electron correlations to be strong in these materials. They should play an important role in model Hamiltonian studies of the TM halides.

As a consequence of $U/W > 1$, one may expect rich correlation phenomena such as magnetic order, Mott-insulating phases, etc. For instance, in contrast to experimental results[46, 47] showing insulating behavior in VI_3 , the partially filled bands in PBE calculations give rise to a half-metallic behavior[50, 51]. This implies that electron-electron interactions play a crucial role in electronic and magnetic properties of TM halides, especially in the systems with nearly half-filled $3d$ bands. Applying the DFT+ U method with $U=3.8$ eV to MnX_2 dihalides not only increases the band gap but also results in ferromagnetic order, whereas these systems remain antiferromagnetic when calculated without U [41]. In the case of VI_3 , DFT+ U employing $U=3.5$ eV opens a finite band-gap of about 0.84 eV [50], which is in agreement with experiments, while the system is a half-metal within DFT-PBE. VI_3 is therefore commonly classified as a Mott insulator. This inconsistency between experiment and DFT-PBE has also been found for CrX_3 , manifesting a possible Mott insulating state[31, 36]. Experimentally, CrI_3 is insulating[24, 25, 28] even above the Curie temperature, which suggests that the band-gap does not stem from the exchange splitting (i.e., from magnetism) but that the strong electron-electron correlation is responsible for the formation of the band gap in this material. There are theoretical works that argue that the band gap of Cr-based trihalides can be described as a mixture of Mott-Hubbard and charge-transfer type[36]. Note that layered materials that exhibit a Mott-insulating character are very rare. The Mott phase has been experimentally discovered in bilayer twisted graphene[69–71], $\sqrt{13} \times \sqrt{13}$ supercell of 1T-TaS(Se) $_2$ and 1T-NbSe $_2$ materials (the Star of David cluster)[72–74], and TM phosphorous trichalcogenides[75], MPX_3 , where M is a TM and X are chalcogen elements, which were confirmed by *ab initio* calculations [71, 76, 77]. In all mentioned monolayers, the observed insulating phase has been discussed to originate from the presence of narrow bands around the Fermi energy. For example, in the distorted phase of 1T-TaS $_2$, there is a flat band with mainly d_{z^2} character at E_F which increases U/W sub-

stantially [78–80], even though the Coulomb interaction parameter U has been calculated to be 0.4 eV only [80], which is significantly smaller than the corresponding value $U=2.27$ eV in undistorted 1T-TaS₂ [81]. Such narrow bands, of t_{2g} or e_g character, are also present in CrI₃, VI₃, and NiI₂, resulting in a large U/W difference between TM halides and elementary TMs.

IV. SUMMARY AND OUTLOOK

We have performed systematic *ab initio* calculations to determine the strength of the effective Coulomb interaction (Hubbard U) between localized electrons in various 2D TM Halides with formulas MX_2 and MX_3 ($M=Ti, V, Cr, Mn, Fe, Co, Ni$; $X=Cl, Br, I$) employing the parameter-free cRPA scheme. We found that in most of the metallic TM halides (in the non-magnetic state) the Hubbard U parameters for t_{2g} or e_g electrons are larger than 3.0 eV, and the band widths W are less than 1.0 eV. As a consequence, we find that $U/W > 1$. So, these materials can be classified as moderately to strongly correlated systems. The correlation strength in TM halides is much larger than the corresponding values in elementary TMs and TM compounds. Furthermore, using the calculated U and J values we discuss the stability of the ferromagnetic ordering within the Stoner model. The obtained Coulomb interaction parameters are important both for a basic understanding of the physics of TM halides and for use in model Hamiltonians applied to describe electronic, magnetic, and optical properties of these materials.

The ferromagnetic state of MX_3 compounds can undergo thermal and quantum fluctuations. The thermal fluctuations are relevant to all of them. This provides a nice experimental handle to study the role of the underlying magnetic background in transport and other properties by tuning the temper-

ature across the Curie temperature. This is a unique opportunity not present in generic two-dimensional materials. For the compounds with small magnetic moment, the quantum fluctuations are expected to play a significant role. The effective theory of small fluctuations around a magnetically ordered state is known as non-linear sigma model [82]. They describe spin-1 bosons known as magnons. Such bosons can mediate forces between the electrons, pretty much the same way gauge bosons (photons) mediate the Coulomb interactions. The part of the interaction mediated by spin-1 bosons cannot be screened [83]. Therefore our MX_3 compounds having smaller magnetic moments are expected to display many unexpected correlation phenomena, such as non-Fermi liquids. The present paradigm for study of correlation physics in 2D systems, unlike high temperature superconductors or heavy fermion systems are not buried in the bulk, but live in a true 2D layer. They can therefore enjoy most of the control and functionalization methods developed in the context of graphene [84].

Furthermore, in analogy to graphene nanoribbons [85] where armchair ribbons offer low-energy one-dimensional bands, the nanoribbons of TM halides are expected to serve as a new platform for strongly correlated one-dimensional bands. Such bands are spatially separated from the other bands, and hence the fascinating Luttinger physics can be studied using local probes. Also gapping out the edge modes in such ribbons [86] in the present correlated systems can be an interesting framework for electronic applications that require an energy gap, albeit with substantial Mott character.

Acknowledgements

E.S. and I.M. gratefully acknowledge funding provided by the European Union (EFRE, Project No. ZS/2016/06/79307).

-
- [1] A. K. Geim and K. S. Novoselov, Nat. Mater. **6**, 183 (2007).
 - [2] M. I. Katsnelson, Mater. Today **10**, 20 (2007).
 - [3] Han, W., Kawakami, R. K., Gmitra, M. and Fabian, J., Nat. Nanotechnol. **9**, 794–807 (2014).
 - [4] H. Ohno, D. Chiba, F. Matsukura, T. Omiya, E. Abe, T. Dietl, Y. Ohno, and K. Ohtani, Nature **408**, 944 (2000).
 - [5] M. Ashton, D. Gluhovic, S. B. Sinnott, J. Guo, D. A. Swartz, and R. G. Hennig Nano Lett. **17**, 5251 (2017).
 - [6] E. Şaşıoğlu, S. Blügel, and I. Mertig, ACS Appl. Electron. Mater. **1**, 1552 (2019)
 - [7] N. D. Mermin and H. Wagner, Phys. Rev. Lett. **17**, 1133 (1966).
 - [8] J. O. Sofo, A. S. Chaudhari, and G. D. Barber, Phys. Rev. B **75**, 153401 (2007).
 - [9] E. Şaşıoğlu, H. Hadipour, C. Friedrich, S. Blügel, and I. Mertig, Phys. Rev. B **95**, 060408(R) (2017).
 - [10] D. W. Boukhvalov, M. I. Katsnelson, and A. I. Lichtenstein, Phys. Rev. B **77**, 035427 (2008).
 - [11] D. C. Elias, R. R. Nair, T. M. G. Mohiuddin, S. V. Morozov, P. Blake, M. P. Halsall, A. C. Ferrari, D. W. Boukhvalov, M. I. Katsnelson, A. K. Geim, and K. S. Novoselov, Science **323**, 610 (2009).
 - [12] J. Zhou, Q. Wang, Q. Sun, X. S. Chen, Y. Kawazoe, and P. Jena, Nano Lett. **9**, 3867 (2009).
 - [13] O. V. Yazyev and L. Helm, Phys. Rev. B **75**, 125408 (2007).
 - [14] H. Hadipour, Phys. Rev. B **99**, 075102 (2019).
 - [15] M. M. Ugeda, I. Brihuega, F. Guinea, and J. M. Gomez-Rodriguez, Phys. Rev. Lett. **104**, 096804 (2010).
 - [16] K. M. McCreary, A. G. Swartz, W. Han, J. Fabian, and R. K. Kawakami, Phys. Rev. Lett. **109**, 186604 (2012).
 - [17] R. R. Nair, M. Sepioni, I-Ling Tsai, O. Lehtinen, J. Keinonen, A. V. Krasheninnikov, T. Thomson, A. K. Geim, and I. V. Grigorieva, Nat. Phys. **8**, 199 (2012).
 - [18] S. S. Rao, S. N. Jammalamadaka, A. Stesmans, V. V. Moshchalkov, J. v. Tol, D. V. Kosynkin, A. Higginbotham-Duque, and J. M. Tour, Nano Lett. **12**, 1210 (2012).
 - [19] G. Zsolt Magda, X. Jin, I. Hagymasi, P. Vancso, Z. Osvath, P. Nemes-Incze, C. Hwang, L. P. Biro, and L. Tapasztó, Nature (London) **514**, 608 (2014).
 - [20] H. Feldner, Z. Y. Meng, T. C. Lang, F. F. Assaad, S. Wessel, and A. Honecker, Phys. Rev. Lett. **106**, 226401 (2011).
 - [21] X. Li, X. Wang, L. Zhang, S. Lee, and H. Dai, Science **319**, 1229 (2008).

- [22] H. Hadipour, E. Şaşıoğlu, F. Bagherpour, C. Friedrich, S. Blügel, and I. Mertig, *Phys. Rev. B* **98**, 205123 (2018).
- [23] Ch. Gong, L. Li, Zh. Li, H. Ji, A. Stern, Y. Xia, T. Cao, W. Z. Q. Qiu, R. J. Cava, Steven G. Louie, J. Xia, and X. Zhang, *Nature* **546**, 265–269 (2017).
- [24] B. Huang, G. Clark, E. Navarro-Moratalla, D. R. Klein, R. Cheng, K. L. Seyler, D. Zhong, E. Schmidgall, M. A. McGuire, D. H. Cobden, W. Yao, Di Xiao, P. Jarillo-Herrero, and X. Xu, *Nature* **546**, 270 (2017).
- [25] K. L. Seyler, D. Zhong, D. R. Klein, Sh. Gao, X. Zhang, B. Huang, E. Navarro-Moratalla, L. Yang, D. H. Cobden, M. A. McGuire, W. Yao, D. Xiao, P. Jarillo-Herrero, and X. Xu, *Nature Physics* **14**, 277 (2018).
- [26] D. Shcherbakov, P. Stepanov, D. Weber, Y. Wang, J. Hu, Y. Zhu, K. Watanabe, T. Taniguchi, Zh. Mao, W. Windl, J. Goldberger, M. Bockrath, Ch. N. Lau, *Nano Lett.* **18**, 4214 (2018).
- [27] B. Shabbir, M. Nadeem, Zh. Dai, M. Fuhrer, Q. K. Xue, X. Wang, Q. Bao, *Applied Physics Reviews* **5**, 041105 (2018).
- [28] Sh. Jiang, L. Li, Z. Wang, K. F. Mak, and J. Shan, *Nature Nanotechnology*, **13**, 549 (2018).
- [29] M. Bonilla, S. Kolekar, Y. Ma, H. C. Diaz, V. Kalappattil, R. Das, T. Eggers, H. R. Gutierrez, M. H. Phan and M. Batzill, *Nature Nanotechnology* **13**, 289 (2018).
- [30] D. J. OHara, T. Zhu, A. H. Trout, A. S. Ahmed, Y. K. Luo, Ch. H. Lee, M. R. Brenner, S. Rajan, J. A. Gupta, D. W. McComb, and R. K. Kawakami, *Nano Lett.* **18**, 3125 (2018).
- [31] Michael A. McGuire, Hemant Dixit, Valentino R. Cooper, and Brian C. Sales *Chem. Mater.* **27**, 612 (2015).
- [32] Ping Li, *Phys. Chem. Chem. Phys.* **21**, 6712 (2019).
- [33] Sh. Tomar, B. Ghosh, S. Mardanya, P. Rastogi, B. S. Bhadoria, Y. S. Chauhan, A. Agarwal, and S. Bhowmick, *Journal of Magnetism and Magnetic Materials*, **489**, 165384 (2019).
- [34] H. Wang, V. Eyert, and U. Schwingenschlogl, *J. Phys.: Condens. Matter*, **23** 116003 (2011).
- [35] L. Webster, L. Liang, and J. A. Yan, *Phys. Chem. Chem. Phys.*, **20**, 23546 (2018).
- [36] Wei-Bing Zhang, Qian Qu, Peng Zhua, and Chi-Hang Lam, *J. Mater. Chem. C*, **3**, 12457 (2015).
- [37] Wei-xi Zhang, Yong Li, Hui Jin, and Yan-chao She, *Phys. Chem. Chem. Phys.*, **21**, 17740 (2019).
- [38] Michael A. McGuire, *Crystals* **7**, 121, (2017).
- [39] A. S. Botana and M. R. Norman, *Phys. Rev. Materials* **3**, 044001 (2019).
- [40] Junjie He, Xiao Li, Pengbo Lyu and Petr Nachtigall, *Nanoscale*, **9**, 2246 (2017).
- [41] Vadym V. Kulish and Wei Huang, *J. Mater. Chem. C*, **5**, 8734 (2017).
- [42] M. A. McGuire, G. Clark, S. KC, W. M. Chance, G. E. Jellison, V. R. Cooper, X. D. Xu, and B. C. Sales, *Phys. Rev. Mater.*, **1**, 014001 (2017).
- [43] Zh. Zhang, J. Shang, Ch. Jiang, A. Rasmita, W. Gao and T. Yu, *Nano Lett.* **19**, 5, 3138-3142 (2019)
- [44] M. C. De Siena, S. E. Creutz, A. Regan, P. Malinowski, Q. Jiang, K. T. Kluherz, Gu. Zhu, Zh. Lin, J. J. De Yoreo, X. Xu, J. H. Chu, and D. R. Gamelin, *Nano Lett.* **20**, 3, 2100-2106 (2020).
- [45] T. Kurumaji, S. Seki, S. Ishiwata, H. Murakawa, Y. Kaneko, and Y. Tokura, *Phys. Rev. B* **87**, 014429 (2013).
- [46] S. Son, M. J. Coak, N. Lee, J. Kim, T. Y. Kim, H. Hamidov, H. Cho, Ch. Liu, D. M. Jarvis, Ph. A. C. Brown, J. H. Kim, Ch. H. Park, D. I. Khomskii, S. S. Saxena, and J. G. Park, *Phys. Rev. B* **99**, 041402(R) (2019)
- [47] T. Kong, K. Stolze, E. I. Timmons, J. Tao, D. Ni, S. Guo, Z. Yang, R. Prozorov and R. J. Cava, *Adv. Mater.*, **31**, 1808074 (2019).
- [48] O. Besbes, S. Nikolaev, N. Meskini, and I. Solovyev, *Phys. Rev. B* **99**, 104432 (2019).
- [49] I. V. Solovyev, *J. Phys.: Condens. Matter* **20**, 293201 (2008).
- [50] Sh. Tian, J. F. Zhang, Ch. Li, T. Ying, Sh. Li, X. Zhang, K. Liu, and H. Lei, *J. Am. Chem. Soc.* **141**, **13**, 5326-5333 (2019).
- [51] J. He, Sh. Ma, P. Lyua, and P. Nachtigall, *J. Mater. Chem. C*, **4**, 2518 (2016).
- [52] J. Liu, Q. Sun, Y. Kawazoed and P. Jenac, *Phys. Chem. Chem. Phys.*, **18**, 8777 (2016).
- [53] D. Torelli, K. S. Thygesen, and T. Olsen, *2D Mater.* **6**, 045018 (2019).
- [54] E. Şaşıoğlu, C. Friedrich, and S. Blügel, *Phys. Rev. B* **83**, 121101(R) (2011).
- [55] H. Hadipour and Y. Yekta, *Phys. Rev. B* **100**, 195118 (2019).
- [56] F. Aryasetiawan, M. Imada, A. Georges, G. Kotliar, S. Biermann, and A. I. Lichtenstein, *Phys. Rev. B* **70**, 195104 (2004); F. Aryasetiawan, K. Karlsson, O. Jepsen, and U. Schönberger, *Phys. Rev. B* **74**, 125106 (2006); T. Miyake, F. Aryasetiawan, and M. Imada, *Phys. Rev. B* **80**, 155134 (2009).
- [57] E. Şaşıoğlu, C. Friedrich, and S. Blügel, *Phys. Rev. B* **83**, 121101(R) (2011).
- [58] Y. Nomura, M. Kaltak, K. Nakamura, C. Taranto, S. Sakai, A. Toschi, R. Arita, K. Held, G. Kresse, and M. Imada, *Phys. Rev. B* **86**, 085117 (2012); B-C. Shih, Y. Zhang, W. Zhang, and P. Zhang, *Phys. Rev. B* **85**, 045132 (2012).
- [59] N. Marzari and D. Vanderbilt, *Phys. Rev. B* **56**, 12847 (1997).
- [60] F. Freimuth, Y. Mokrousov, D. Wortmann, S. Heinze, and S. Blügel, *Phys. Rev. B* **78**, 035120 (2008).
- [61] <http://www.flapw.de>
- [62] J. P. Perdew, K. Burke, and M. Ernzerhof, *Phys. Rev. Lett.* **77**, 3865 (1996).
- [63] A. A. Mostofi, J. R. Yates, Y.-S. Lee, I. Souza, D. Vanderbilt, and N. Marzari, *Comput. Phys. Commun.* **178**, 685 (2008).
- [64] C. Friedrich, S. Blügel and A. Schindlmayr, *Phys. Rev. B*, **81**, 125102 (2010).
- [65] Y. O. Kvashnin, A. Bergman, A. I. Lichtenstein, and M. I. Katsnelson, *Phys. Rev. B* **102**, 115162 (2020).
- [66] V. I. Anisimov, I. V. Solovyev, M. A. Korotin, M. T. Czyzyk, and G. A. Sawatzky, *Phys. Rev. B* **48**, 16929 (1993).
- [67] V. Anisimov and Y. Izyumov, *Electronic Structure of Strongly Correlated Materials*, Springer Berlin Heidelberg (2010).
- [68] G. Stollhoff, A. M. Oles, and V. Heine, *Phys. Rev. B* **41**, 7028 (1990).
- [69] Ch. Shen, Y. Chu, Q. Wu, N. Li, Sh. Wang, Y. Zhao, J. Tang, J. Liu, J. Tian, K. Watanabe, T. Taniguchi, R. Yang, Z. Yang Meng, D. Shi, O. V. Yazyev, and G. Zhang, *Nat. Phys.* (2020).
- [70] K. Seo, V. N. Kotov, and B. Uchoa, *Phys. Rev. Lett.* **122**, 246402 (2019).
- [71] Y. Choi, J. Kemmer, Y. Peng, A. Thomson, H. Arora, R. Polski, Y. Zhang, H. Ren, J. Alicea, G. Refael, F. V. Oppen, K. Watanabe, T. Taniguchi, and S. Nadj-Perge, *Nature Physics* **15**, 1174 (2019).
- [72] L. Ma, Cu. Ye, Y. Yu, X. F. Lu, X. Niu, S. Kim, D. Feng, D. Tomanek, Y. Son, X. H. Chen, and Y. Zhang, *Nature Communications* **7**, 10956 (2016).
- [73] L. Perfetti, A. Georges, S. Florens, S. Biermann, S. Mitrovic, H. Berger, Y. Tomm, H. Hochst, and M. Grioni, *Phys. Rev. Lett.* **90**, 16 (2003).
- [74] T. Ritschel, J. Trinckauf, K. Koepf, B. Büchner, M. v. Zimmermann, H. Berger, Y. I. Joe, P. Abbamonte, and J. Geck, *Nature Physics* **11**, 328 (2015).
- [75] S. Y. Kim, T. Y. Kim, L. J. Sandilands, S. Sinn, M. Ch. Lee, J. Son, S. Lee, K. Y. Ch, W. Kim, B. G. Park, C. Jeon, H. D. Kim,

- Ch. H. Park, J. G. Park, S. J. Moon, and T. W. Noh, Phys. Rev. Lett. **120**, 136402 (2018).
- [76] H. Kim, K. Haule, and D. Vanderbilt, Phys. Rev. Lett. **123**, 236401 (2019).
- [77] S. H. Lee, J. S. Goh, and D. Cho, Phys. Rev. Lett. **122**, 106404 (2019).
- [78] C. Tresca and M. Calandra, 2D Mater. **6**, 035041 (2019).
- [79] P. Darancet, A. J. Millis, and C. A. Marianetti, Phys. Rev. B **90**, 045134 (2014).
- [80] E. Kamil, J. Berges, G. Schonhoff, M. Rosner, M. Schuler, G. Sangiovanni, and T. O. Wehling, J. Phys.: Condens. Matter **30**, 32 (2018).
- [81] M. Cococcioni and S. de Gironcoli, Phys. Rev. B **71**, 035105 (2005).
- [82] E. Fradkin, *Field Theories of Condensed Matter Physics*, Cambridge Univ. Press, New York, 2013
- [83] A. M. Tsvelik, *Quantum Field Theory in Condensed Matter Physics*, Cambridge Univ. Press, New York, 2003
- [84] M. I. Katsnelson, *Graphene*, Cambridge Univ. Press, New York, 2012
- [85] L. Brey and H. A. Fertig, Phys. Rev. B **73**, 235411 (2006).
- [86] Young-Woo Son, Marvin L. Cohen, and Steven G. Louie Phys. Rev. Lett. **97**, 216803 (2007).